Catalysis Science & Technology

Accepted Manuscript

This is an *Accepted Manuscript*, which has been through the Royal Society of Chemistry peer review process and has been accepted for publication.

Accepted Manuscripts are published online shortly after acceptance, before technical editing, formatting and proof reading. Using this free service, authors can make their results available to the community, in citable form, before we publish the edited article. We will replace this *Accepted Manuscript* with the edited and formatted *Advance Article* as soon as it is available.

You can find more information about *Accepted Manuscripts* in the Information for Authors.

Please note that technical editing may introduce minor changes to the text and/or graphics, which may alter content. The journal's standard Terms & Conditions and the Ethical guidelines still apply. In no event shall the Royal Society of Chemistry be held responsible for any errors or omissions in this *Accepted Manuscript* or any consequences arising from the use of any information it contains.

ROYAL SOCIETY OF CHEMISTRY

www.rsc.org/catalysis

Journal Name

ARTICLE

Sulfur-resistant and regenerable Ni/Co spinel-based catalysts for methane dry reforming

S.T. Misture,[a] K.M. McDevitt,[a] K.C. Glass,[a] D.D. Edwards,[a] J.Y. Howe,[b] K.D. Rector,[c] H. He[c] and S.C. Vogel[c]

Received 00th January 20xx,
Accepted 00th January 20xx

DOI: 10.1039/x0xx00000x

www.rsc.org/

Oxide-supported metal catalysts were prepared by thermal impregnation of highly crystalline and highly-faceted starting spinels of the form $(M_{0.75}Mg_{0.25})Al_2O_4$, where M = Ni, Co, or Cu and mixtures thereof. *In-situ* reduction at 900°C extracts the transition metals from the oxide, and the resulting catalysts contain metal crystallites with particle sizes of ~100 nm and exceedingly low dispersion, but show high activity for dry reforming of methane with turnover frequencies as large as 3.9 at 850°C. The $Ni_{0.375}Cu_{0.375}Mg_{0.25}Al_2O_4$ catalyst shows stable methane conversion out to 12 hours on stream without performance-degrading coking. For the Ni/Co catalysts, the reforming activity and sulfur tolerance are both functions of the Ni/Co ratio and the synthesis temperature of the starting spinel, with $Ni_{0.375}Co_{0.375}Mg_{0.25}Al_2O_4$ synthesized at 1500°C displaying fast reaction kinetics even in the presence of 20 ppm H_2S. High reforming activity is attributed to long linear lengths of high-perfection facet edges and corners on the metal crystallites. Sulfur tolerance appears to be improved by a combination of the oxygen storage capacity of the defective spinel support and its faceting that provides additional reaction sites for activation of CO_2.

A. Introduction

Methane reforming is of great current interest given the broad availability of abundant methane supplies. However, while steam reforming is a commercially attractive process for hydrogen production, a recent study shows that dry reforming of methane (DRM) is not competitive with steam reforming.[1] Nonetheless, dry reforming remains of high interest for processing CO_2 into useful products, notably syngas, for many commercial processes.

General agreement exists regarding the degradation mechanisms of Ni based catalysts under dry reforming conditions and for fuel streams that contain sulfur. Although oxidative carbon removal mechanisms have been documented, the details of sulfur tolerance, as well as rational design approaches to link the metal and support chemistries to the poisoning behaviors, remain elusive. High activity Ni and Co spinels have recently been studied for DRM, with the $NiAl_2O_4$ spinel support yielding higher catalyst stability than Fe-Co or Ce-Ni-Al supports.[2] Using Raman spectroscopy, the authors attribute the high stability to the formation of only non-deactivating carbon species. Similarly, Nikolla and coworkers[3] found that 1 wt.% Sn partitions to the surface of Ni and strongly improves carbon tolerance by reducing the binding energy of carbon on the undercoordinated surface sites. With respect to sulfur, literature shows that sulfur poisoning of Ni-based catalysts can be largely reversed at temperatures in excess of ~800°C simply by removing the sulfur source.[4] Additions of Co to Ni-based catalysts have been effective in improving sulfur tolerance,[5] and it is clear that approaches to reduce the formation of oxy- and metal-sulfides or to discover new catalysts that function even in the presence of these surface contaminants would have a large impact on dry reforming of especially biofuels.

Most recently, combination of high reactivity metals with oxide supports that facilitate oxygen transport has shown promise. For example, Wang and coworkers[6] synthesized mesoporous Ni-Ce-Al catalysts that showed high DRM activity and good stability, with turnover frequencies (TOFs) reaching 1.2 s^{-1} at 800°C. A clear link between metal dispersion and TOF demonstrated that the mesoporous nature of the support was effective in reducing sintering, while the high oxygen mobility of the CeO_2 promoter improved activation and reduction of CO_2 to reduce coking.

Spinels of the form AB_2O_4 have been studied for DRM and steam reforming of methanol, and they have been recognized for some time as regenerable by oxidation (see for example reviews [7, 8]). Spinel catalyst supports are typically synthesized using wet chemical methods, yielding nanoscale powders that are later wet impregnated. An alternate approach, one of 'thermal impregnation,' involves selective reduction of transition metal cations from the parent oxide leaving the remnant oxide as the catalyst support.[9-11]

The crystal chemistry of the spinels used in thermal impregnation reactions is relevant to the surface acid/base character, oxide ion transport, and surface adsorption sites. In addition to the chemistry, the spinel structure is defined by the lattice parameter (a), the inversion parameter (*i*), and the anion parameter (u). Inversion refers to the occupancy of the tetrahedral site (one site per formula unit) by the majority cation B, with *i* equivalently defined $(A_{(1-i)}B_i)(A_iB_{(2-i)})O_4$). Inversion has been shown

[a] Kazuo Inamori School of Engineering, Alfred University, Alfred, NY 14802
[b] Materials Science and Technology Division, Oak Ridge National Laboratory, Oak Ridge, Tennessee 37831
[c] Manuel Lujan Jr. Neutron Scattering Center, Los Alamos National Laboratory, Los Alamos, NM 87545, USA

† Footnotes relating to the title and/or authors should appear here.
Electronic Supplementary Information (ESI) available: [details of any supplementary information available should be included here]. See DOI: 10.1039/x0xx00000x

This journal is © The Royal Society of Chemistry 20xx

Please do not adjust margins

Catalysis Science & Technology Accepted Manuscript

to be an equilibrium function of many factors, including temperature, composition, pressure, ionic charge, ionic radii, crystal and ligand field effects, and anion polarization.[12]

The anion parameter, u, is defined as the fractional coordinate for x=y=z=u for the anion. Typical values for the anion parameter are between 0.24 and 0.275. An oxygen parameter u = 0.25 yields a perfectly close-packed oxygen sublattice, with any deviation from 0.25 giving a less closely packed sublattice. As u increases above 0.25, the tetrahedral site is enlarged at the expense of the octahedral site.[13] The anion parameter varies such that the volumes of the tetrahedral and octahedral interstices match the volume of each ion.

Spinels also accommodate some non-stoichiometry. Of relevance to the surface acid/base character, $MgAl_2O_4$ dissolves excess MgO and Al_2O_3, with the total extent of dissolution of MgO lower and requiring higher temperatures; MgO dissolution starts at 1800 °C.[14] Al_2O_3 dissolution is charge compensated by cation vacancies, distributed on both octahedral and tetrahedral sites,[15] and possibly by a small number of oxygen vacancies as well.[16] Al_2O_3 dissolution is possible beginning at 700 °C, with $MgO{\cdot}2Al_2O_3$ stable at 1600 °C, and $MgO{\cdot}4Al_2O_3$ stable at 1800 °C. $NiAl_2O_4$ does not dissolve excess NiO, but can dissolve excess Al_2O_3, though to a lesser degree than $MgAl_2O_4$.

After forming the spinel, gas-phase reduction may be used to effect "thermal impregnation,"[11] that is, extraction of the reducible cation(s) from the oxide. Our earlier work showed that the reduction reaction for $Ni_xMg_{1-x}Al_2O_4$ proceeds by removal of both oxygen and Ni ions from the oxide, and the remnant spinel approaches the γ-Al_2O_3 structure, according to equation 1.[17] In addition, we previously showed [17] that the remnant spinel becomes unstable at temperatures in excess of ~1000°C, and transforms to the higher transition aluminas.

$$Ni_xMg_{1-x}Al_2O_4 \rightarrow xNi + Mg_{(1-x)\left(\frac{4}{4-x}\right)}Al_{2\left(\frac{4}{4-x}\right)}O_4 \qquad (1)$$

The present paper demonstrates the use of highly crystalline, low surface area and low dispersion Ni/Co spinel catalysts with excellent activity for DRM and good sulfur resistance. We exploit the flexibility of the spinel chemistry to include Mg in the starting spinel to yield a remnant spinel support with chemistry approaching $MgAl_2O_x$. In addition, choice of synthesis temperature defines the extent of crystal faceting of the oxide support, which influences the metal crystallization and defines the catalyst performance. The new catalysts can be oxidatively regenerated to completely reverse sulfur poisoning.

B. Methods

Catalysts were prepared using solid state methods as reported earlier[17] at compositions listed in Table 1 and heat treated from 1200 to 1600°C in air. Pellets were gently crushed to yield large granules suitable for catalyst testing. Off-line reductions were performed under pure H_2 at ambient pressure or at reduced pressure of 300 Torr.

XRD patterns were collected in reflection geometry with a Bruker D8 Advance diffractometer using Cu Kα radiation and a position-sensitive Lynxeye detector. The metal content of the reduced spinels was determined using Rietveld analysis for quantification, as reported earlier[17], and these values were used in the estimations of turnover frequency (TOF).

In-situ neutron powder diffraction was performed at Los Alamos National Laboratory using the High-Pressure-Preferred-Orientation (HIPPO) powder diffractometer[18] with the sample heated in the ILL furnace. The ILL furnace was appropriately modified to accommodate a gaseous environment around the sample via a silica glass gas envelope. The gas envelope was pumped and backfilled with H_2, then heated at 5 K/min to the isothermal hold temperature of 950°C. Data sets were collected in increments of 5.2 minutes during heating and upon reaching 950°C, and the sample was held isothermally for 2 hours before cooling to room temperature. Rietveld refinements of the neutron powder diffraction data were performed using GSAS (General Structure Analysis System)[19] and its graphical interface EXPGUI[20] using the modified von Dreele neutron time-of-flight profile function (GSAS function #1 for neutron time of flight data).[21]

Catalyst reforming activity was measured in a fixed-bed reactor at the Technical University of Munich and at Nexceris, Inc. For the former, the catalyst was conditioned at 900°C before running the reaction. Reaction conditions were as follows: 850°C, 10 bar, with flow of 100 ml/min and feed gas composition of 47.5% CH_4, 47.5% CO_2, 5% N_2. The new catalyst was compared to a reference Pt on ZrO_2 reforming catalyst.

Reactivity, sulfur poisoning and catalyst regeneration were measured using a separate system, using ~0.25g catalyst sample (0.2 mL volume) in a fixed-bed reactor with total flow rate of 200 mL/min. The sample was reduced under hydrogen at 900°C prior to cooling to the reaction temperature of 850°C for isothermal measurements or 650°C for non-isothermal measurements. Reactivity and sulfur poisoning were tested using a gas composition of 32.5% CH_4, 64.5% CO_2 3.0% N_2 and gas hourly space velocity (GHSV) = 60,000 hr^{-1} (50,000 ml/h/g catalyst) with or without 20 ppm H_2S. Catalyst regeneration included switching the fuel stream to air and oxidizing the catalyst for 2 hours, followed by re-reducing at 900°C and continuing the test at 850°C. Samples were cooled in the same gas and oxidized only upon removal from the system at room temperature.

Microscopy was performed using an Hitachi NB5000 FIB-SEM to prepare cross-sections of powder grains, and TEM was performed using an Hitachi HF3300. SEM imaging was performed using a Zeiss Merlin instrument. Metal grain sizes were estimated from SEM images using the line intersection method, with 100 grains measured from several photographs.

C. Results and Discussion

Parent spinel

Table 1 summarizes the samples prepared and tested, which include varied chemistry of the spinel A site. After synthesis at 1300°C or higher all materials contained four phases, the spinel, two polymorphs of zirconia, and what is likely a trace amount of NiO identified tentatively using one barely-detectable XRD peak. While long heat treatments at 1100 and 1200°C yielded a majority spinel phase, binary oxide impurities remained. The added 2.5 wt. % ZrO_2 crystallizes as a combination of monoclinic and tetragonal zirconia, as shown by small XRD peaks shown in a representative Rietveld refinement shown in Fig. 1. Mg^{2+} is a well-known stabilizer for ZrO_2, and presumably stabilizes the tetragonal polymorph.

Figure 2 shows the microstructure of $Ni_{0.5}Co_{0.5}Al_2O_4$ after synthesis at 1300 and 1600°C, providing a qualitative indication that the crystallites grow and develop more faceting as the synthesis temperature increases. The high crystal perfection of samples synthesized at and above 1300°C limits the accuracy of XRD peak broadening analysis but we find that the crystallite size derived from full-pattern Rietveld fitting is 0.34(5) and 0.51(7) μm for

Catalysis Science & Technology Accepted Manuscript

This journal is © The Royal Society of Chemistry 20xx

Please do not adjust margins

samples heated to 1300 and 1500°C. In addition to changes in the faceting and annealing of defects, we anticipate some changes in the spinel inversion parameter (*i*) to occur with temperature. It is widely accepted that the degree of inversion for $NiAl_2O_4$ decreases with increasing temperature as Ni^{2+} cations preferentially shift from the octahedral to the tetrahedral sites.[22]

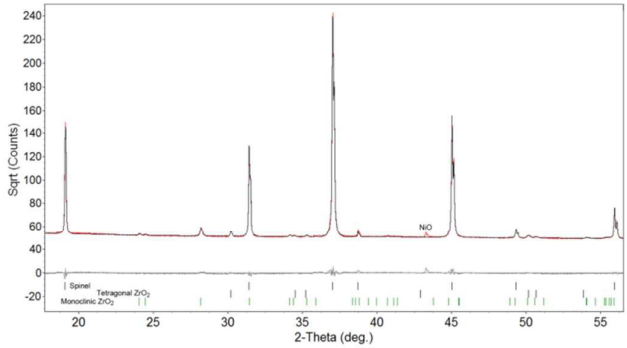

Figure 1: Rietveld refinement of the XRD data.

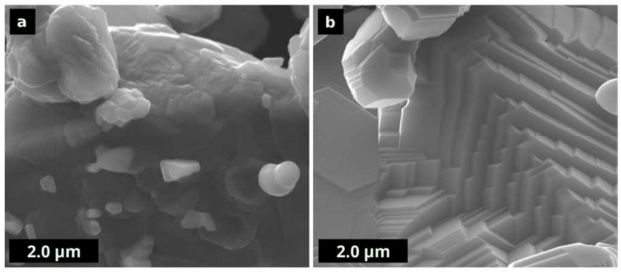

Figure 2: SEM micrographs of $Ni_{0.5}Co_{0.5}Al_2O_4$ after synthesis at (a) 1300°C and (b) 1600°C.

Figure 3 shows SEM images of the Ni, Co, and Cu-containing spinels synthesized at 1500°C. The powder grains are characterized by a high degree of well-developed faceting for all chemistries. The faceting develops such that the catalyst grains present primarily {111} faces as defined by perfect equilateral triangular faces and corner-truncated triangular faces.[23] The microstructure of the Cu containing sample is largely octahedra composed of {111} facets. For the Ni and Co containing samples, the {111} character is also dominant but some {110} and {100} forms are also present.

D.For {111} facets, and ignoring surface reconstruction, the terminations for a spinel with some degree of inversion may be: (1) a negatively charged oxygen layer; (2) a non-planar, positively-charged metal atom layer with both tetrahedral and octahedral A and B cations; or (3) a positively-charged octahedral metal layer. The nature of the surface termination is important in the function of the catalyst, but so is the presence of facet step edges. Several experimental and theoretical studies have probed the question of surface reconstruction in $MgAl_2O_4$ spinel. Although the specific reaction conditions will influence the active mechanisms, the surface polarity is likely to be satisfied by formation of surface oxygen vacancies and/or adsorption of charge-balancing ions. For the {111} facets of $MgAl_2O_4$ recent work shows that the surface accommodates ~40% oxygen vacancies and/or facilitates strong dissociative adsorption of water, depending on the conditions.[24-26] While the microstructures display mainly {111} facets, the crystallites tend to form truncated octahedra with extensive {111} {100} intersections with an interplanar angle of 54.7°.

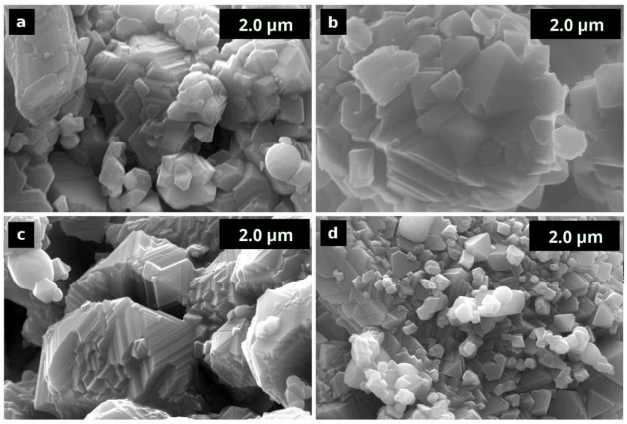

Figure 3: Secondary electron photomicrographs of as-synthesized spinels. (a) $Ni_{0.75}Mg_{0.25}Al_2O_4$, (b) $Cu_{0.375}Ni_{0.375}Mg_{0.25}Al_2O_4$, (c) $Co_{0.675}Ni_{0.075}Mg_{0.25}Al_2O_4$, (d) $Co_{0.375}Ni_{0.375}Mg_{0.25}Al_2O_4$.

Reduction reactions

Upon high temperature reduction to effect thermal impregnation, the zirconia phases remain unchanged and the remnant oxide phase retains the spinel structure for temperatures below 1000°C. In parallel, metal crystallites form primarily on the surfaces of the oxide grains.

Figure 4 shows the microstructures for granular materials after reduction at 750, 850, and 900°C. As highlighted in Fig. 4(a) and (b), the surface microstructure of the spinel phase, with extensive faceting, is unchanged during reduction. Figure 4(b) shows a high magnification image wherein we find facets on the spinel which appear flat and smooth at low magnification in fact contain many small step edges (<10 nm) that become only faintly visible at the highest achievable SEM magnification.

At lower reduction temperatures, Fig.4 (a) and (b), few Ni grains are present and they display roughly spherical symmetry with apparently random locations on the oxide grains. By 850°C (Fig. 4(c)) we find that self-organization of the Ni grains occurs where the Ni grains preferentially nucleate at – or diffuse to – facet step edges. Of particular interest, we note in the bottom right corner of Fig. 4(c) Ni grains formed at all 3 apices of a 111 triangular facet, suggesting that the Ni nucleates at highly undercoordinated sites on the oxide surface. In addition, Figure 4(c) shows that the Ni grains preferentially grow with one elongated axis with approximately square cross-section, and with precise crystallographic registry to the facets on the spinel support. Although we expect the equilibrium crystal shape to be bounded by low-index {111} and {100} facets, as is the case for most FCC metals, [27] the Ni crystallites take on highly anisotropic shapes when reduced from the oxide at 850°C. While the reduction temperature of 850°C is well below the melting temperature of 1455°C, we attribute the non-equilibrium shape primarily to registry of the Ni atomic planes with the spinel crystal structure, as shown later using TEM.

Reduction at 900°C causes notable changes in both the spinel support and the Ni grains. As additional Ni and oxygen are extracted from the spinel, further reduction in unit cell volume occurs,[17, 28] and surface cracks and crevices form along preferred crystallographic directions (Fig. 4(d)).

From Fig. 4, it is also clear that enhanced Ni mobility with increasing temperature causes Ni crystallite growth and the habit of the crystals changes from elongated to equiaxed when the crystals

Catalysis Science & Technology Accepted Manuscript

are on the free surfaces. The crystallites in Fig. 4(d) lodged in the facet step edges maintain their anisotropic shapes, while those on free surfaces develop towards the equilibrium shape. As shown in Fig. 4(d), the average size of the Ni crystallites is between 50 and 100 nm and each Ni grain appears to be monocrystalline without aggregation. Furthermore, the Ni grains have well-developed facets with sharp edges at both the Ni-Ni facet intersections and at the Ni-spinel interfaces. The faceting remains dominated by {111} faces with sharp angles between adjacent faces – often less than 120° – providing a long length of well-ordered undercoordinated sites as well as well-ordered interfaces between the metal and oxide support. Nagaoka and coworkers[29, 30] demonstrated that oxygen transfer at the metal-ZrO_2 interface is critical for oxidative sulfur removal in ZrO_2-suppported Ni catalysts, but little is known about the effects of crystal orientation and local interfacial nanostructures on oxygen transfer. As discussed later, higher crystal perfection and faceting improve sulfur tolerance in the Ni-Co catalysts.

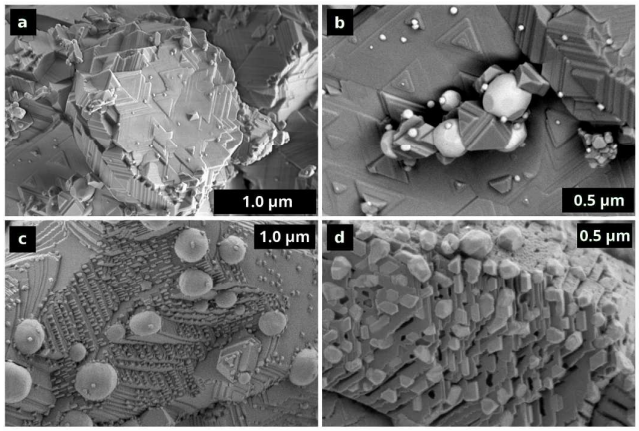

Figure 4: SEM images of $Ni_{0.75}Mg_{0.25}Al_2O_4$ + 2.5 wt.% ZrO_2 after synthesis at 1500°C and reduction under H_2 at (a and b) 750°C; (c) 850°C; and (d) 900°C.

Extraction of oxygen and nickel from the spinel lattice results in a volumetric strain that is relieved by surface cracking as shown in Fig. 4. The present study of microcrystalline spinel catalysts allows careful characterization of the spinel structure and inversion which is not straightforward with nanocrystalline spinel supports. An *in-situ* neutron powder diffraction study was undertaken in an attempt to quantify any oxygen deficiency in the remnant spinel, to better understand if the defect spinel might accommodate facile oxygen or hydroxyl exchange during reforming. Figure 5 shows a representative Rietveld refinement for one *in-situ* diffraction pattern during reduction for a sample of composition $Ni_{0.75}Mg_{0.25}Al_2O_4$. The presence of diffraction peaks from two spinel phases demonstrates that the reaction proceeds via nucleation and growth, without an oxygen-and cation-deficient intermediate form, likely in a core-shell geometry where the external surfaces of grains reduce first, followed by the core.

The behaviors of the lattice parameter and the oxygen positional parameter as a function of time, also shown in Fig. 5, provide new information about the remnant spinel catalyst support. It has been well established that the degree of inversion in $NiAl_2O_4$ is a function of temperature and composition.[22] During reduction, removal of Ni and oxygen causes contraction of the lattice and re-distribution of the Al cations within the crystal. The lattice contraction is expected because the larger Ni^{2+} cation is removed, along with oxygen ions. Rietveld refinements of the neutron diffraction data clearly show that the oxygen sublattice remains fully occupied after the reduction reaction, demonstrating that lattice reconstruction during reduction expels oxygen vacancies to the surfaces of the crystallites while Al is redistributed to form the non-stoichiometric remnant spinel. As a consequence, we find not only that surface cracks develop in the spinel support (Fig. 4) but that the surface cracking pattern follows the crystallography. Although diffusion in non-stoichiometric spinels remains a topic of some debate, the surface cracking patterns indicate anisotropic diffusion coefficients. In stoichiometric Mg-Al spinels, diffusion of hydrogen is known to be at least an order of magnitude faster than the diffusion of any other species in the spinel, and self-diffusion of oxygen is the slowest.[31] Therefore, the rate limiting step in the reduction reaction is either diffusion of nickel, oxygen/hydroxyl, or both, assuming that any change in the spinel inversion by Al redistribution is much faster than bulk mass transport.

The oxygen positional parameter (*u*) is indicative of the extent of spinel inversion; as the *u* value increases above 0.25 the tetrahedral site is enlarged at the expense of the octahedral site. The inset in Fig. 5 shows that the *u* parameter decreases with time during reduction, meaning that the inversion decreases as result of removal of the larger Ni^{2+} cation from the octahedral sites in the structure.

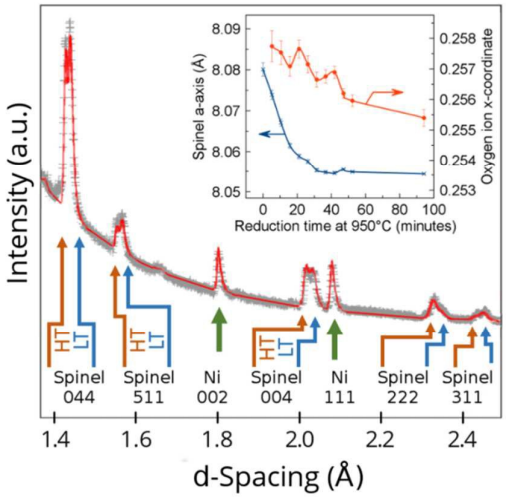

Figure 5: Rietveld refinement of *in-situ* neutron powder diffraction pattern of $Ni_{0.75}Mg_{0.25}Al_2O_4$ collected at 900°C under 4% H_2. LT and HT indicate the low temperature and high temperature spinel phases. Inset shows the refined lattice constant and oxygen ion *u*-coordinate with error bars of ± 1 standard deviation.

The ZrO_2 phases, which are present as the monoclinic and tetragonal polymorphs, form roughly spherical particles with only subtle faceting as shown in Fig. 4(b). Several facets are present on the otherwise generally spherical crystals, suggesting that the synthesis temperature (1500°C) is near but somewhat below the crystal roughening temperature for ZrO_2. Ni grains are present on the ZrO_2 crystals, but perhaps more importantly, Ni grains collect at the interface between the ZrO_2 and spinel. The microstructure therefore presents boundaries of four phases where spinel, zirconia, nickel and the gas phase intersect. As discussed later, it is possible that this complex multi-phase boundary plays a role in activation of the reactants or oxidative removal of sulfur.

Attempts to prepare cross-sections via focused ion beam milling were unsuccessful in maintaining the subtle surface

Catalysis Science & Technology Accepted Manuscript

This journal is © The Royal Society of Chemistry 20xx

Please do not adjust margins

features, but were useful to show that the Ni grains nucleate and grow with crystallographic registry to the oxide spinel. As shown in Fig. 6, the orientations of several adjacent Ni grains are identical, demonstrating that the Ni preferentially grows from the oxide with primarily {111} exposed facets, with some {110} and {100} terminations. This behavior is also noted in Fig. 4(d) where parallel alignment of the Ni grains on different facet steps is evident, while both images in Fig. 6 show that the Ni crystallites present a large linear density of {111} faces intersecting {100} faces at 54.7°.

Figure 6 shows the catalyst after testing at 10 bar for 20 hours; comparing the images in Figs. 4 and 6 shows that the microstructure of the catalyst after testing remains similar to that of the fresh catalyst, ignoring the whisker carbon. Powder XRD was used to estimate the Ni crystallite size before and after catalyst testing at 850°C for 20h, and indicated that some Ni crystallite growth occurred. Values of 76(6) and 105(12) nm were obtained from analysis of the Ni XRD peaks from samples before and after catalyst testing, respectively. Ni crystallite sizes measured from SEM images similar to that in Fig. 6(b) provide an estimate of the crystallite size of 119 nm with standard deviation of 44 nm, in reasonable agreement with the XRD result of 105(12) nm.

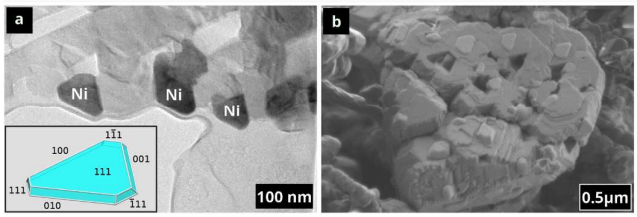

Figure 6: (a) TEM of FIB cross-section of $Ni_{0.75}Mg_{0.25}Al_2O_4$ + 2.5 wt.% ZrO_2 after synthesis at 1500°C and reduction under H_2 at 900°C. (b) SEM image of the same catalyst after 20 hours on stream at 10 bar.

Catalytic activity

Reduction of the catalyst at 900°C followed by 20 hours on stream under 10 bar with 1:1 CH_4:CO_2 ratio yields the results in Fig. 7. The spinel catalyst conversions for CH_4 and CO_2 initially decrease for ~3h, and then increase gradually throughout the remaining 17 hours. The yields follow a similar trend, and the selectivity towards CH_4 and CO_2 decrease slightly in the initial 200 minutes and remain stable thereafter. Post-situ SEM observation (Fig. 6) shows the presence of whisker-like carbon and additional coking which did not degrade the performance. The carbon was evaluated using Raman spectroscopy, and the presence of both graphitic and disordered carbon was noted (see Fig. 8). The well-known D (disordered carbon, 1357 cm^{-1}) and G (graphitic carbon, 1588 cm^{-1}) bands [32] were detected, **where the intensity of the G band was 4.5 times larger than that of the D band**. Therefore, the coking yields primarily graphitic carbon but nonetheless both the methane and CO_2 conversions *increased* with time from 3 to 20 hours on stream, without causing pressure drop across the reactor.

The Ni crystals, which are terminated almost entirely by flat, low-index facets, appear to offer fewer active sites for strong carbon bonding, or at least provide a sufficient density of high-activity sites to maintain the overall high conversions with graphitic carbon present. It is known that carbon is more stable on high-index steps than on flat terraces[33] and therefore we surmise that carbon forms primarily on the relatively small number of step edges present on the Ni crystals. A small quantity of graphitic carbon may therefore be a primary cause of the initial drop in catalyst activity, with maturation of the catalyst microstructure after a few hours increasing the activity while the graphitic carbon remains present.

The high reactivity of the Ni/spinel catalyst in comparison to Pt/ZrO_2 suggests that the low-dispersion Ni does not reduce the kinetics of methane activation. It is clear from the microstructures that the Ni grains present highly-ordered and well-defined undercoordinated sites for gas-phase reactions where the facets are flat to within a few nanometers and facet edges and corners are exceedingly sharp with linear lengths of tens of nanometers. Such microstructures are fundamentally different than those of nanoscale (<20 nm) particles formed by wet impregnation. The facet corners are highly undercoordinated and both the facet corners and edges are spatially well-separated from the spinel support, at least in comparison to wet-impregnated catalysts with metal particles of 10 nm or smaller. Furthermore, the large-grained Ni catalysts have large areas of low-index planes exposed to the reaction environment, thus reducing the number density of step edges compared to nanoscale Ni but providing large flat terraces for reaction. It has been established by studies on single crystals that methane decomposition is most rapid on Ni(110), followed by Ni(100) and Ni(111).[34] Although it is not trivial to quantify the area density of each type of crystallographic facet, additional work is underway to better understand how the large Ni grains facilitate high methane activation kinetics.

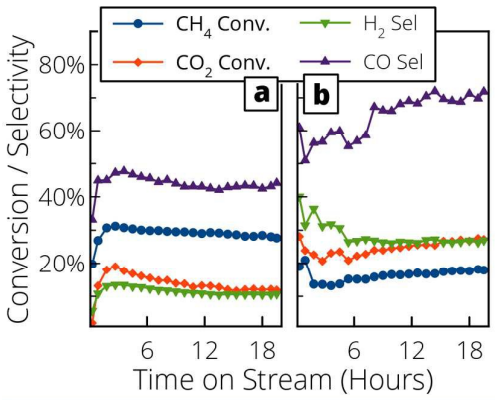

Figure 7: Catalysis testing results under 10 bar, 47.5% CH_4, 47.5% CO_2, 5% N_2 for (a) reference Pt/ZrO_2 catalyst; (b) $Ni_{0.75}Mg_{0.25}Al_2O_4$ synthesized at 1500°C.

Activation of CO_2 is also critical in the reaction kinetics and oxidative carbon removal, and a recent report shows that nanoscale $MgAl_2O_4$ activates CO_2 via formation of carbonate, bidentate, and formate species.[35] For the defective spinels with starting chemistry $(Ni,Mg)Al_2O_4$, most of the Ni is removed during the reduction reaction, but the remnant spinel should retain its propensity towards strong CO_2 adsorption because it retains the Mg ions. Furthermore, the defective spinel support, containing a majority of {111} facets and therefore some 40% surface oxygen vacancies, is expected to accommodate enhanced oxygen, OH^-, or proton transfer.[24] Additionally, the ZrO_2 particles allow facile oxygen transport, and likely improve the CO_2 activation and reduction, at least locally, to aid carbon removal.

Catalyst testing in a different reactor at 1 bar and 850°C with 1:1 CO_2:CH_4 ratio demonstrated high reactivity, but formation of whisker carbon for Ni, Co and Ni/Co containing samples. The Cu/Ni catalyst showed some coking (see Figs. 8 and 9) but no degradation in catalytic activity or drop in flow rate with time out to 12 hours on stream. Kim, Rodriguez and Baker[36] have shown that carbon

Catalysis Science & Technology Accepted Manuscript

diffusion through the metal catalyst is the rate limiting step for filament carbon growth. As the transport of carbon through the metal particle is slowed, the reaction favors a coating of non-deactivating amorphous carbon, evidenced by the relatively stronger graphitic peak in nickel samples versus nickel-copper alloys.

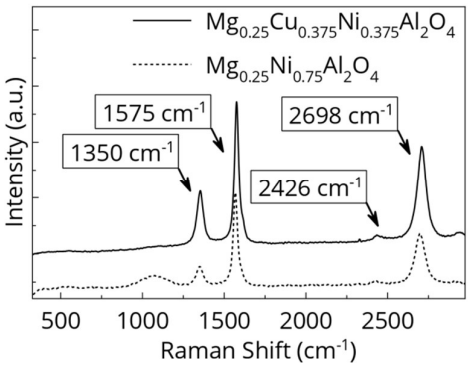

Figure 8: Raman spectra for Ni and Cu-based catalysts after 18 and 12 hours on stream, respectively at 1:1 CO_2:CH_4 ratio.

The Ni and Co containing catalysts reach CH_4 conversion rates well above 90% for the same conditions, but form excessive whisker carbon. The reduction of the conversion rate by a factor of slightly more than two for the benefit of improved coking behavior represents a dramatic improvement over an earlier report[37] showing that the CH_4 conversion for nanoscale $CuAl_2O_4$ is 50 times lower than that of $NiAl_2O_4$.

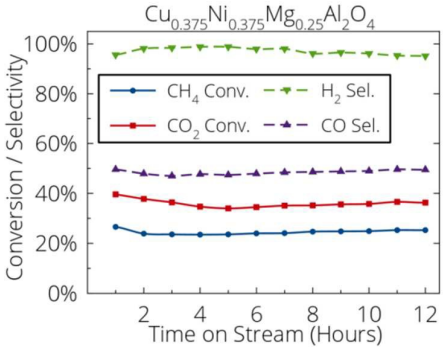

Figure 9: Catalytic activity of a Cu-containing catalyst under 1:1 CO_2:CH_4 ratio.

To explore further the Ni, Co and Ni/Co catalysts, additional testing was performed with 2:1 CO_2:CH_4 ratio. The temperature response of the reaction rates is shown in Fig. 10 for two (Ni,Mg)Al_2O_4 samples, one processed at 1300°C and one processed at 1500°C. As noted earlier, the catalyst synthesized at higher temperature shows fewer crystalline defects and larger coherent diffracting domain size, with more defined crystal faceting. The reaction rates are similar between the two samples, though the reaction is likely limited by reactant flow at the highest temperature of 850°C.

The influences of Mg, Ni and Co in varied concentrations were examined by measuring the reaction rates and the results are captured in Table 1. Although some of the samples reach 100% conversion indicating that the reactant flow is limiting, the results demonstrate high reaction rates for all of the Ni-based catalysts. Additions of Co up to 67% of the total A-site content results in decreased reaction rates with the highest initial methane conversion of 97% for the 1:1 Ni:Co ratio. Table 1 also shows the change in reaction rate with time on stream, where $Ni_{0.375}Cu_{0.375}Mg_{0.25}Al_2O_4$ improved by nearly 5% with time and $Ni_{0.5}Co_{0.5}Al_2O_4$ degraded by ~5% over the 16 hour duration.

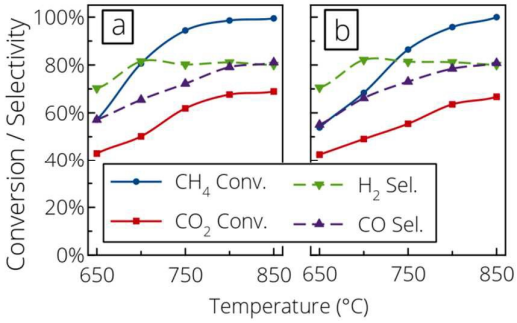

Figure 10: Methane reforming results for $Ni_{0.75}Mg_{0.25}Al_2O_4$ catalysts synthesized at (a) 1300°C and (b) 1500°C. Reaction conditions: 650-850°C, 32.5% CH_4, 64.5% CO_2, 3.0% N_2 and GHSV = 60,000 hr^{-1}.

Table 1: Reaction rates and degradation for the catalysts tested.

Composition	**%CH_4 Conversion at t=0 and (steady state)**	H_2 Selectivity	Change in CH_4 conversion (%, time)
1:1 CO_2:CH_4, 1 bar, 850°C			
$Ni_{0.375}Cu_{0.375}Mg_{0.25}Al_2O_4$	**27 (25)**	95.1 (12h)	-7.4 (12h)
$Ni_{0.75}Mg_{0.25}Al_2O_4$	**96 (N/A)**	92 (3h)	-3.2 (3h)
2:1 CO_2:CH_4, 1 bar, 850°C			
$Ni_{0.75}Mg_{0.25}Al_2O_4$	**100 (100)**	79 (16h)	0 (16h)
$NiAl_2O_4$	**100 (100)**	80 (16h)	0 (16h)
$Ni_{0.5}Co_{0.5}Al_2O_4$	**97 (92)**	80 (16h)	-5.3 (16h)
$Ni_{0.375}Co_{0.375}Mg_{0.25}Al_2O_4$	**75 (N/A)**	80 (0h)	N/A
$Ni_{0.075}Co_{0.675}Mg_{0.25}Al_2O_4$	**49 (N/A)**	85 (0h)	N/A

Assuming that dissociative adsorption of methane is rate-limiting,[6] the TOF values and apparent activation energies were calculated for the reactions as a function of temperature using the uncorrected methane conversions. Figure 11 shows the TOF vs. reciprocal temperature, and demonstrates that high TOF values are attained. TOF value at 650°C is 2.3, and the TOF increases to 3.9 at 850°C. Such high values have been occasionally documented for Ni based catalysts, with Pt catalysts generally having lower TOF values of <2. For comparison, mesoporous Ni-based catalysts with Ce-Al supports reach TOF = 1.2 at 800°C with metal particles sizes smaller than 10 nm. Interestingly, a recent report comparing Ni and Pt catalysts shows that a Ni catalyst on α-Al_2O_3 with 25 nm crystallites reaches TOF = 3.7 at 550°C.[38] The catalysts described herein have particle sizes four times larger, but similarly large TOFs, suggesting that a unique feature of the metal crystallites and/or oxide support improves the reaction rate. We attribute the large reaction rate to the high-perfection facet edges, which provide large linear densities of atomically-defined 'step edges' for methane reaction.[39] In other words, the total metal surface area appears to be less important than the availability of well-defined reaction sites for dissociative adsorption of methane. Direct characterization of the adsorption is non-trivial, but additional work is in progress to identify the critical microstructural features that result in high TOFs.

Catalysis Science & Technology Accepted Manuscript

This journal is © The Royal Society of Chemistry 20xx

Please do not adjust margins

The apparent activation energies (E_a) for the reaction are similar between the $Ni_{0.75}Mg_{0.25}Al_2O_4$samples prepared at 1300°C and 1500°C, 32.0 and 32.5 kJ/mol, respectively. These values lie at the low end of the range of values reported for DRM, 29 – 360 kJ/mol.[6, 40] As noted by Akpan and coauthors,[40] the catalyst support has a dramatic effect on E_a. It is unlikely that the rate controlling step is altered in these Ni-based catalysts, and that the low E_a result from differences in concentration of reaction intermediates facilitated by the nature of the support.

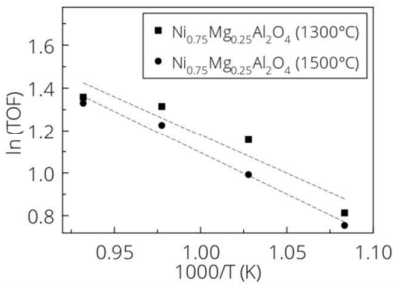

Figure 11: Arrhenius plot of TOF values for $Ni_{0.75}Mg_{0.25}Al_2O_4$ catalysts prepared at 1300 and 1500°C.

Regeneration and sulfur tolerance

For temperature excursions below 1000°C, we find that the spinel reduction and reoxidation reactions are completely reversible. In-situ XRD, reported earlier,[17] showed that the initial reduction reaction results in the formation of Ni grains accompanied by a decrease in the spinel unit cell volume. Subsequent re-oxidation reverses the reaction, but includes NiO as the first reaction product, which later reacts with the remnant spinel to recover the initial spinel.

During catalyst regeneration, mechanical and microstructural integrity is paramount for recovering high catalytic activity. In-situ XRD and post-mortem SEM indicate that no changes occur in the phase assemblages or microstructures of the catalysts after redox cycling. Figure 12 shows the in-situ SEM, demonstrating that reoxidation occurs even in the microscope at $pO_2 \sim 10^{-9}$ atm. Most critically, no changes in the parent spinel faceting or grain size were noted at temperatures up to 1200°C, promising high stability in reforming reactions at <900°C.

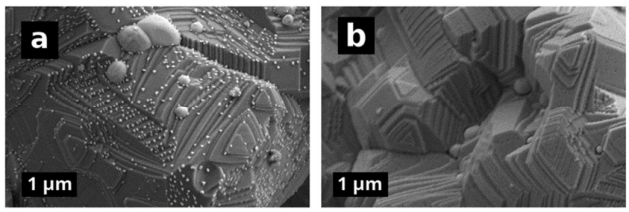

Fig. 12: *In-situ* SEM of $NiAl_2O_4$. (a) sample at RT after reduction at 900°C for 1h under 1 atm. H_2. (b) *In-situ* image captured immediately upon reaching 1200°C after heating at 30 K/min.

The addition of H_2S to the feed gas at 850°C had a negative effect on the catalytic activity, but highlighted differences among the Ni/Co ratios and sintering temperatures. Figure 13 shows the results for the $Ni_{0.75}Mg_{0.25}Al_2O_4$ catalysts prepared at 1300 and 1500°C, suggesting that higher crystal perfection and faceting improves sulfur tolerance and that CO_2 interactions with highly undercoordinated facet edge sites is the likely mechanism improving the oxidative sulfur removal.

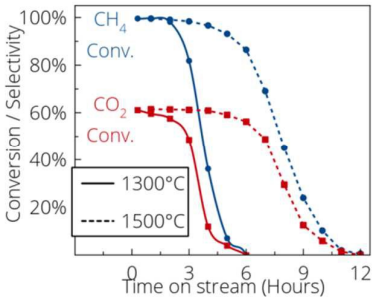

Figure 13: Effect of H_2S on methane reforming performance over $Ni_{0.75}Mg_{0.25}Al_2O_4$ catalysts with low faceting (1300°C synthesis) and high faceting (1500°C synthesis) under conditions of 850°C, 20 ppm H_2S, 29.3% CH_4, 58.1%CO_2, 12.6% N_2 and GHSV = 60,000 hr^{-1}.

Except for $Ni_{0.375}Co_{0.375}Mg_{0.25}Al_2O_4$ with 2.5 wt.% ZrO_2, all of the catalysts showed decreases in CH_4 conversion to below 10% within 10 hours. $Ni_{0.375}Co_{0.375}Mg_{0.25}Al_2O_4$ with 2.5 wt.% ZrO_2, however, showed lower but stable conversion of ~40% from 8-12 hours under sulfur poisoning conditions. Regeneration of the catalysts dramatically improved the initial performance and in all cases re-set the catalyst to the initial activity level, an example of which is shown in Fig. 14. This result is in contrast to earlier work where regeneration of Al_2O_3-suppported Ni was ineffective for reversing sulfur poisoning when the oxidation was carried out at 700°C.[4] In fact, these authors speculated that $NiAl_2O_4$ was formed during the oxidation stage. From their results, it appears that Ni reduction from the spinel was apparently kinetically limited at 700°C, precluding formation of new Ni crystallites and recovery of the catalytic activity.

Regeneration of $Ni_{0.375}Co_{0.375}Mg_{0.25}Al_2O_4$ with 2.5 wt.% ZrO_2, in contrast, improved the catalytic performance while maintaining the good sulfur resistance. Improved performance via regeneration is likely a result of maturation of the microstructure. The surface cracking that occurs upon reduction (shown schematically in Fig. 14) is unlikely to recover completely during re-oxidation, and formation of additional surface cracking after the second reduction may enhance the surface area and improve the metal dispersion. The data in Fig. 14 show that the initial CH_4 conversion of 94% decreased by only 4% over 12 hours under 20 ppm sulfur, pointing to enhanced oxidative sulfur removal.

Few other reports regarding sulfur tolerance in Ni catalysts for dry reforming are available. A recent study on dry reforming of H_2S-containing biogas [5] empirically showed that MgO and ZrO_2 promoters, as well as additions of Co to the Ni-based catalysts, improved activity for biogas reforming. Furthermore, these authors reported that Co additions to Ni (*i.e.* 5%Co/15%Ni) improved the sulfur tolerance, though no mechanisms were proposed.

Two factors are identified in the present work as relevant to improved sulfur tolerance: the sintering temperature (or in other words the perfection and faceting of the starting spinel) and the Co content. It is generally known that Co-Ni bimetallic catalysts show high methane reforming activity, and that appropriate additions of Co to Ni can reduce coking.[41] The Ni/Co ratio is critical to avoid Co oxidation and excessive coking. The former occurs when the oxygen produced by CO_2 activation is consumed too slowly by oxidation of

Catalysis Science & Technology Accepted Manuscript

adsorbed carbon from CH_4 activation, and the latter occurs at high Co loading because of the increased reaction rate.

Little is known about the mechanisms of sulfur removal during the DRM reaction. Quantum mechanical calculations have shown that the energy for H_2S adsorption onto metallic surfaces is slightly higher for Co than for Ni, and hence Co should be more prone to sulfur poisoning.[42] The observation herein of higher sulfur tolerance for the catalyst synthesized at the highest temperature points to improved CO_2 activation on the more highly-faceted spinel support to enhance oxidative sulfur removal. This mechanism parallels that of coking resistance in Ni/ZrO_2, where Nagaoka and coworkers showed that the ZrO_2 support facilitates CO_2 activation and the resulting oxygen is exchanged at the metal/ZrO_2 interface to gasify adsorbed carbon species.[29, 30] In the case of Ni/ZrO_2, the variable valence of Zr and facile formation of oxygen vacancies are key to the presence of active oxygen species. For the spinel-supported catalyst of the form $(Co_{0.375}Ni_{0.375}Mg_{0.25})Al_2O_4$, some Ni and Co remain in the remnant spinel after the reduction reaction at 900°C and the remnant spinel is highly defective.[17] The point defects created by extraction of most of the Ni/Co/Cu and approximately 18% of the oxygen ions (*i.e.* ~0.75 oxygen ions out of 4 per formula unit) may facilitate oxygen storage and transfer because the lattice is unlikely to relax to a defect-free state during reduction. The redox reaction of $Co^{2+/3+}$ in the remnant spinel may provide additional oxygen vacancies for storage of active oxygen or it may have some minor influence the surface reconstruction. Recent experimental work on Co_3O_4 spinel shows that the surface polarity on {111} terminations is equilibrated by inversion of Co ions to optimize the $Co^{2+/3+}$ charge balance.[43] As discussed earlier, the surface reconstruction and adsorbed species are likely to have a large impact on the reaction kinetics. Experimental and theoretical work shows that the {111} facets of $MgAl_2O_4$ accommodate ~40% oxygen vacancies and/or facilitate strong dissociative adsorption of water, depending on the conditions.[24-26] The additional oxygen available at the metal-spinel interface may in turn oxidize surface adsorbed sulfur atoms during operation

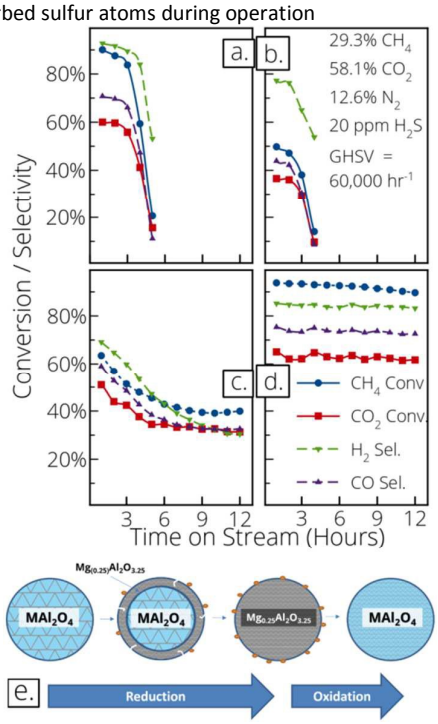

Figure 14: Initial sulfur poisoning data for (a) $Ni_{0.75}Mg_{0.25}Al_2O_4$; (c) $Ni_{0.375}Co_{0.375}Mg_{0.25}Al_2O_4$. (b) and (d) are the catalyst performance after regenerating samples from (a) and (c), respectively. (e) shows a schematic of the microstructure maturation process.

D. Conclusions

Microcrystalline spinel-supported Ni, Ni-Co and Ni-Cu catalysts were successfully prepared at high temperatures to provide highly faceted oxides and the metal was extracted from the oxide by reduction at 900°C. The resulting low-dispersion, microcrystalline catalysts may be considered a midpoint between nanoscale wet-impregnated catalysts and single crystal surfaces.

The Ni and Ni-Co catalysts show high reaction kinetics characterized by TOFs reaching 3.9 at 850°C and low activation energies of ~32 kJ/mol with metal particle of ~120 nm. High activity with low dispersion is attributed to the large linear length of highly undercoordinated sites at metal facet edges that act like high-index step edges in nanocrystalline Ni catalysts. Sulfur tolerance was linked to the synthesis temperature and hence crystal perfection and extent of equilibrium crystal faceting. The Ni/Co ratio also had a dramatic impact on sulfur resistance. While additional work is underway to firmly establish the mechanisms of sulfur removal, the results suggest that the defective spinel oxide improves oxygen storage and supply during CO_2 activation, similar to the oxygen ion conductors ZrO_2 and CeO_2. Improved faceting probably also provides more reaction sites on the oxide support for CO_2 activation, and the large area of reconstructed {111} facets may increase oxygen transfer. Oxygen diffusion to the metal facet edges, corners, and step edges is proposed to oxidatively remove sulfur. Regeneration of the catalysts was proven effective to reverse sulfur poisoning, and in one instance, for $Ni_{0.375}Co_{0.375}Mg_{0.25}Al_2O_4$, the CH_4 conversions under 20 ppm H_2S decreased by only 4% during 12 hours on stream.

Acknowledgements

This material is based upon work supported by the National Science Foundation under Grant CBET-1033810. The authors thank: L. A. Schulz, A. Jentys and J. A. Lercher of the Technical University of Munich for performing the catalyst activity testing shown in Fig. 7; P. Pedersen of Carl Zeiss Microscopy, LLC for images in Fig. 4 (a) and (b); and B.E. Hill at Alfred University for preparing the first sample for catalyst testing. The SEM portion of this research was conducted at the Center for Nanophase Materials Sciences, which is sponsored at Oak Ridge National Laboratory by the Scientific User Facilities Division, Office of Basic Energy Sciences, U.S. Department of Energy. This work made use of the Raman spectrometer at the Cornell Center for Materials Research Shared Facilities which are supported through the NSF MRSEC program (DMR-1120296). This work has benefited from the use of the Los Alamos Neutron Science Center (LANSCE) at the Los Alamos National Laboratory. LANSCE was funded until 2014 by the US Department of Energy under Contract W-7405-ENG-36.

Notes and references

1. S. T. Oyama, P. Hacarlioglu, Y. Gu and D. Lee, *Int. J. Hydrogen Energy*, 2012, **37**, 10444-10450.

Catalysis Science & Technology Accepted Manuscript

This journal is © The Royal Society of Chemistry 20xx

Please do not adjust margins

2. F. F. deSousa, H. S. A. deSousa, A. C. Oliveira, M. C. C. Junior, A. P. Ayala, E. B. Barros, B. C. Viana, J. M. Filho and A. C. Oliveira, *Int. J. Hydrogen Energy*, 2012, **37**, 3201-3212.
3. E. Nikolla, J. Schwank and S. Linic, *J. Catal.*, 2009, **263**, 220-227.
4. M. Ashrafi, C. Pfeifer, T. Proell and H. Hofbauer, *Energy Fuels*, 2008, **22**, 4190-4195.
5. B. Saha, A. Khan, H. Ibrahim and R. Idem, *Fuel*, 2014, **120**, 202-217.
6. N. Wang, K. Shen, L. Huang, X. Yu, W. Qian and W. Chu, *ACS Catalysis*, 2013, **3**, 1638-1651.
7. K. Aasberg-Petersen, I. Dybkjaer, C. V. Ovesen, N. C. Schjodt, J. Sehested and S. G. Thomsen, *J. Nat. Gas Sci. Eng.*, 2011, **3**, 423-459.
8. M.-S. Fan, A. Z. Abdullah and S. Bhatia, *ChemCatChem*, 2009, **1**, 192-208.
9. US20050255995A1, 2005.
10. J. N. Kuhn, Z. Zhao, L. G. Felix, R. B. Slimane, C. W. Choi and U. S. Ozkan, *Applied Catalysis B: Environmental*, 2008, **81**, 14-26.
11. WO2009008955A1, 2009.
12. P. Porta, F. S. Stone and R. G. Turner, *J. Solid State Chem.*, 1974, **11**, 135-147.
13. H. S. C. O'Neill and A. Navrotsky, *Am. Mineral.*, 1983, **68**, 181-194.
14. D. M. Roy, R. Roy and E. F. Osborn, *Am. J. Sci.*, 1953, **251**, 337-361.
15. R. I. Sheldon, T. Hartmann, K. E. Sickafus, A. Ibarra, B. L. Scott, D. N. Argyriou, A. C. Larson and R. B. Von Dreele, *J. Am. Ceram. Soc.*, 1999, **82**, 3293-3298.
16. Y. Okuyama, N. Kurita and N. Fukatsu, *Solid State Ionics*, 2006, **177**, 59-64.
17. B. E. Hill and S. T. Misture, *J. Am. Ceram. Soc.*, 2013, **96**, 3603-3608.
18. H. R. Wenk, L. Lutterotti and S. Vogel, *Nucl. Instrum. Methods Phys. Res., Sect. A*, 2003, **515**, 575-588.
19. A. C. Larson and R. B. V. Dreele, *General Structure Analysis System (GSAS)*, Los Alamos National Laboratory Report LAUR 86-748, 1994.
20. B. H. Toby, *J. Appl. Crystallogr.*, 2001, **34**, 210-213.
21. R. B. Von-Dreele, J. D. Jorgensen and C. G. Windsor, *J. Appl. Crystallogr.*, 1982, **15**, 581-589.
22. J. N. Roelofsen, R. C. Peterson and M. Raudsepp, *American Mineralogist*, 1992, **77**, 522-528.
23. H. S. C. O'Neill, W. A. Dollase and C. R. Ross, II, *Phys Chem Minerals*, 1991, **18**, 302-319.
24. M. K. Rasmussen, K. Meinander, F. Besenbacher and J. V. Lauritsen, *Beilstein Journal of Nanotechnology*, 2012, **3**, 192-197.
25. C. M. Fang, S. C. Parker and G. De With, *J. Am. Ceram. Soc.*, 2000, **83**, 2082-2084.
26. J. H. Harding, *Surf. Sci.*, 1999, **422**, 87-94.
27. H. Meltzman, D. Chatain, D. Avizemer, T. M. Besmann and W. D. Kaplan, *Acta Materialia*, 2011, **59**, 3473-3483.
28. M. E. Miller and S. T. Misture, *J. Phys. Chem. C*, 2010, **114**, 13039-13046.
29. K. Nagaoka, Y. Abe, Y. Hashimoto, T. Ishikawa, K. Sato, Y. Takita, T. Wakatsuki, M. Kunisu, E. Suda and S. Inamoto, *ACS Catalysis*, 2013, **3**, 1564-1572.
30. K. Nagaoka, K. Seshan, J. A. Lercher and K.-I. Aika, *Catal. Lett.*, 2000, **70**, 109-116.
31. J. A. VanOrman and K. L. Crispin, *Reviews in Mineralogy & Geochemistry*, 2010, **72**, 757-825.
32. L. Zhang, L. Li, J. Li, Y. Zhang and J. Hu, *Top. Catal.*, 2014, **57**, 619-626.
33. H. S. Bengaard, J. K. Norskov, J. Sehested, B. S. Clausen, L. P. Nielsen, A. M. Molenbroek and J. R. Rostrup-Nielsen, *J. Catal.*, 2002, **209**, 365-384.
34. T. P. Beebe, D. W. Goodman, B. D. Kay and J. T. Yates, *The Journal of Chemical Physics*, 1987, **87**, 2305-2315.
35. J. Guo, H. Lou and X. Zheng, *Carbon*, 2007, **45**, 1314-1321.
36. M. S. Kim, N. M. Rodriguez and R. T. K. Baker, *J. Catal.*, 1991, **131**, 60-73.
37. A. L. Pinheiro, A. N. Pinheiro, A. Valentini, J. Mendes Filho, F. F. de Sousa, J. R. de Sousa, M. d. G. C. Rocha, P. Bargiela and A. C. Oliveira, *Catal. Commun.*, 2009, **11**, 11-14.
38. F. Pompeo, N. N. Nichio, M. M. V. M. Souza, D. V. Cesar, O. A. Ferretti and M. Schmal, *Appl. Catal., A*, 2007, **316**, 175-183.
39. F. Abild-Pedersen, O. Lytken, J. Engbaek, G. Nielsen, I. Chorkendorff and J. K. Norskov, *Surf. Sci.*, 2005, **590**, 127-137.
40. E. Akpan, Y. Sun, P. Kumar, H. Ibrahim, A. Aboudheir and R. Idem, *Chem. Eng. Sci.*, 2007, **62**, 4012-4024.
41. A. W. Budiman, S.-H. Song, T.-S. Chang, C.-H. Shin and M.-J. Choi, *Catal. Surv. Asia*, 2012, **16**, 183-197.
42. Z. Cheng, J.-H. Wang, Y. Choi, L. Yang, M. C. Lin and M. Liu, *Energy Environ. Sci.*, 2011, **4**, 4380-4409.
43. W. Meyer, K. Biedermann, M. Gubo, L. Hammer and K. Heinz, *Journal of Physics: Condensed Matter*, 2008, **20**, 265011.

Catalysis Science & Technology Accepted Manuscript